Simulation of Self-Image Interference in Single Mode-No-Core-Single Mode Fiber with COMSOL Multiphysics®

Simulation of Self-Image Interference in Single Mode-No-Core-Single Mode Fiber with COMSOL Multiphysics®

Nazirah Mohd Razali, Muhammad Quisar Lokman, Siti Nur Fatin Zuikafly, Fauzan Ahmad, and Hafizal Yahaya

Malaysia-Japan International Institute of Technology, Universiti Teknologi Malaysia, 54100, Kuala Lumpur, Malaysia

Correspondence: nazirahmohdrazali@gmail.com

Abstract. Self-image interference in a single mode-no-core-single mode fiber plays an important role especially for length optimization before acting as a sensor. The interference can be observed through optical simulation software. Past literature has successfully demonstrated the interference via COMSOL Multiphysics®, but the simulation was not restricted to the use of important domains and settings such as perfectly matched layer and surrounding domain causing imprecise simulation results. This paper proposes a simulation of self-image interference in a single mode-no-core-single mode fiber by using the wave-optics module in COMSOL Multiphysics® software. The beam propagation method is used to observe the self-image interference for different self-image indexes ranging from one to four indexes while the self-image length is obtained from the theoretical calculation before a simulation is carried out. The results show that accurate results can be obtained with restricted simulation settings. The number of the self-image index and self-image length produced by the simulation are similar to the calculation. The self-image point is located exactly at the calculated length with a four-decimal point 0.0000 difference, thus overcoming the limitation of the simulated previous work. In the future, the simulation settings and results can be used for reference to simulate the single mode-no-core-single mode fiber structure.

Keywords: Simulation, self-image, single mode-no-core-single mode fiber

1. Introduction

Single mode-no-core-single mode (SNS) fiber has attracted interest in applications as a refractive index (RI) sensor [1-3]. The no-core fiber (NCF) that is sandwiched between the single mode fiber (SMF) plays an important role as a sensing region. Compared to conventional single mode-multimode-single mode (SMS) fiber which used multimode fiber (MMF) as its sensing region [4], SNS exhibits a more sensitive response to the changes in the environment due to the absence of a cladding layer as the fiber itself acts as the core while the external medium acts as the cladding [5]. Instead of modifying the MMF cladding through tapering or wet etching, the NCF sensor can be directly used as a sensor.

When the NCF is sandwiched between the SMF, it provides a unique light propagation known as self-image interference [6, 7]. When light is coupled to an NCF, the modes that are supported by the NCF are excited and the interference between the propagating modes gives rise to an interference pattern along the NCF. At a certain length, light is concentrated along the NCF central axis forming replicas of the self-image. The self-image position is affected by the NCF length so this parameter must be chosen at the self-image point. If the self-image point is located at the output NCF/SMF interface, the minimum

insertion loss and multimode interference (MMI) information can be obtained [1, 8]. However, other self-image points that are after or before this interface will reduce the light intensity coupled to the SMF.

Younus et al. [9] characterized the self-image interference of the SNS structure by using COMSOL Multiphysics® software. However, the author did not emphasize a few domain settings which are compulsory to simulate the SNS structure. Firstly, a surrounding domain is necessary to better imitate actual environments wherein the evanescent wave is exposed to the surrounding medium (air) although no modification is made to the device [6]. Secondly, a perfectly matched layer (PML) is necessary since boundary condition is applied to the simulation [10, 11]. Consequently, the results obtained without considering the actual environment and boundary condition brought about a slightly different calculated and simulated NCF length, indicating imprecision.

In this paper, the SNS structure is simulated via wave optic module-COMSOL Multiphysics® software to observe the self-image interference. We included the surrounding domain and PML in the simulation for improved simulation results. Furthermore, the electric field distribution throughout the SNS is also studied and the underlying physics are discussed.

2. Methodology

2.1 Simulation Approach

The simulation is executed by using commercialized COMSOL Multiphysics 5.5® (COMSOL) software. A two-dimension (2D) space is chosen to simulate the SNS structure instead of a three-dimension (3D) to reduce the difficulty in the meshing process, computer memory usage, and simulation time. The wave optics module is selected to study the electric field distribution and the beam propagation method (BPM) is used to simulate the structure which allows the user to virtually observe the self-image interference when the light propagates through the longitudinal NCF region. BPM has been widely used to demonstrate multimode interference devices for sensing application [1, 11, 12]. In BPM, the user can determine the inference point when analyzing the electric field distribution along the longitudinal SNS structure.

2.2 Geometry Settings

Fig. 1(a) illustrates the typical SNS configuration in 3D. It consists of a short NCF length sandwiched between two SMF. Meanwhile, Fig. 1(b) illustrates the geometry settings of the simulated SNS. It consists of two SMF with core and cladding diameters of 8μm, and 125 μm, respectively. The SMF length is set to 0.1 mm length. The SMF length does not affect the simulation but rather act as a light carrier and to ensure there are input and output light having different diameter from the NCF.

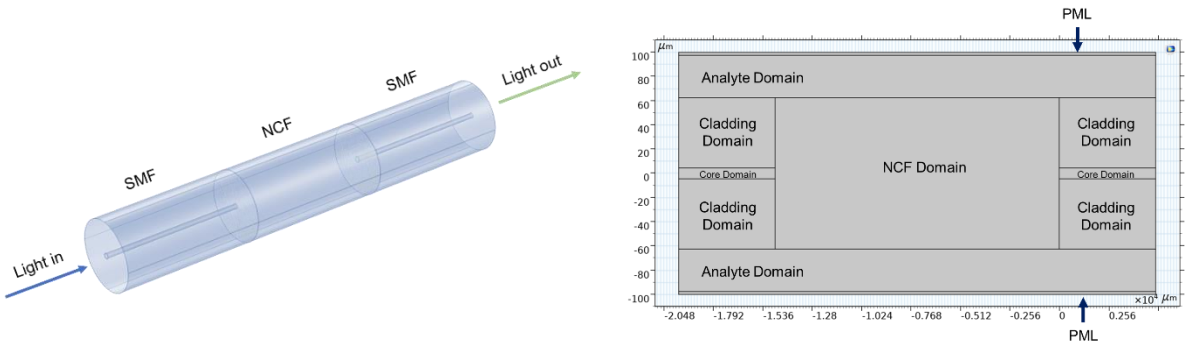

(a) (b)

Fig. 1 The illustration of (a) 3D SNS and (b) 2D SNS for simulation purposes

A simple theoretical calculation is carried out to determine the NCF length as described in Eq. (1) [1, 9]:

$$L = p\frac{n_{NCF}D_{NCF}^2}{\lambda} \tag{1}$$

Where, L is calculated NCF length, p is the self-image index, n_{ncf} is the NCF RI, D is the NCF diameter and λ is the peak wavelength that will replicate the p^{th} image of the input field in an NCF. For a fixed D of 125 μm, n_{ncf} of 1.4440, and λ of 1550 nm, the calculated self-image length is found to be 1.4556 cm, 2.9112 cm, 4.3669 cm, and 5.8225 cm representing one, two, three and four self-image indexes, respectively. The SNS is covered by the analyte domain which represents the analyte medium in actual experiment. Considering the boundary condition for the whole simulation area, PML is added with a thickness of 10 μm as suggested by COMSOL. This highly effective PML is introduced to inhibit spurious reflections from the computational boundaries in the wave propagation model [11]. The geometry settings are summarized as in Table 1.

Table 1 Geometry settings

Parameter	Value
SMF core	8 μm
SMF cladding	125 μm
SMF length	0.1 mm
NCF diameter	125 μm
NCF length	1.4556 cm for one self-image index 2.9112 cm for two self-image indexes 4.3669 cm for three self-image indexes 5.8225 cm for four self-image indexes
PML thickness	10 μm (recommended by COMSOL)

2.3 Refractive Index Settings

A three-term Sellmeier equation is used to express the fiber RI at the near-infrared wavelength region as described in Eq. 2 [13]:

$$n(\lambda) = \sqrt{\frac{A_1\lambda^2}{\lambda^2-\lambda_1^2} + \frac{A_2\lambda^2}{\lambda^2-\lambda_2^2} + \frac{A_3\lambda^2}{\lambda^2-\lambda_3^2} + 1} \tag{2}$$

Where $\boldsymbol{n}$ is the material RI and $\boldsymbol{\lambda}$ is the operating wavelength. Assuming the SMF core is made of 6.3 % of germanium oxide (GeO_2)-doped silica and the cladding and NCF is made from pure silica [13-15], both materials have different Sellmeier coefficients which are shown in the following Table 2.

Table 2 Sellmeier coefficient for simulation [16]

Sellmeier Coefficient	SMF Core	SMF Cladding and NCF
A_1	0.7083925	0.6961663
A_2	0.4203993	0.4079426
A_3	0.8663412	0.8974794
λ_1	0.0853842	0.0684043
λ_2	0.1024839	0.1162414
λ_3	9.8961750	9.8961610

The RI settings are summarized in Table 3. The analyte RI is set 1.0000 RIU, representing the air RI. All the RI medium is set to isotropic. The SMF and NCF are made up from glass and the SNS is assumed to be exposed in the air medium, so they possess only one RI for all directions [17, 18].

Table 3 RI settings

Parameter	Expression	Value
Operating Wavelength	-	1550 nm
SMF core RI	Sellmeier Equation	1.4529 RIU
SMF clad RI NCF RI		1.4440 RIU
Analyte RI	-	1.0000 RIU

3. Results and Discussion

The simulation output is presented in two forms, which are a colored illustration of the electrical field intensity through the SNS structure which helps in visualizing optical properties such as light propagation and self-image interference, and a graph to analyze the electric field distribution and mode field diameter of the simulated device.

Fig. 2 shows the self-image interference along the NCF structure surrounded with air RI of 1.0000 RIU. The number of the self-image increased as the calculated length increased. The electric field distribution shows a few peaks that existed at a point at which the self-image is repeated, representing the interference point. According to Guzman-Sepulveda et. al [6] this result indicates the first clear hint of the typical filter-like spectral response of the SNS sensor.

The results obtained from the simulation are evaluated. SNS relies on the evanescent wave existed at the NCF/analyte boundary to interact with the sensor. In a selective study, Fig. 3 shows the evaluation of the simulated NCF with a length of 5.8225 cm. Fig. 3(a) shows the line to be studied and Fig. 3(b) shows the mode field diameter at the corresponded line. Line 1 and Line 3 represents the destructive and constructive interference, respectively, while Line 2 represents the speckle interference. From Fig. 3(b), there is no evanescent wave existing at the destructive and constructive line. However, the significant evanescent wave can be seen at speckle interference line which proves the speckle-gram interference as a part of multimode interference for sensing applications [19, 20].

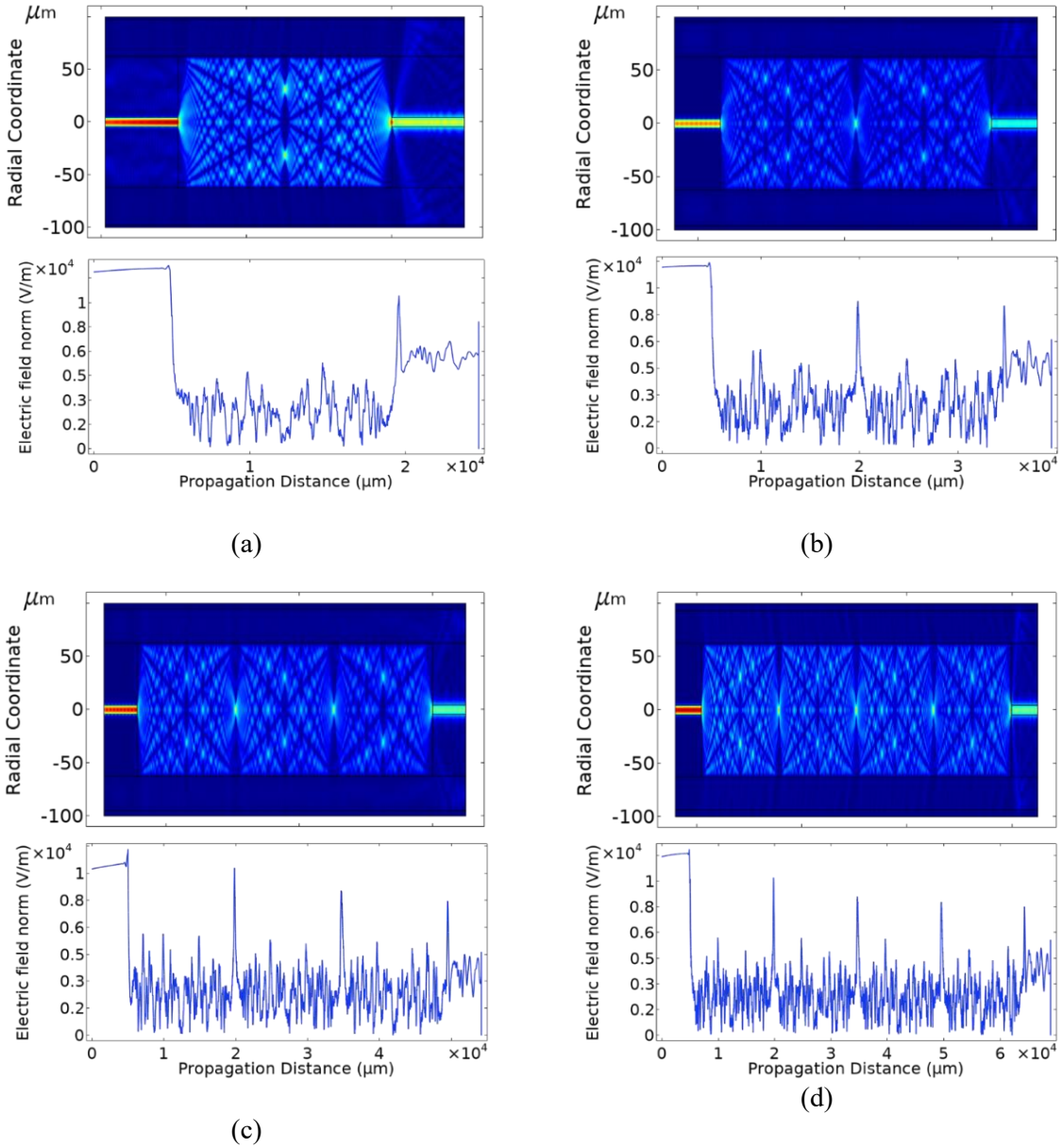

Fig. 2. Light propagation and the electric field distribution of the NCF structure at the calculated self – image length of a) 1.4556 cm, b) 2.9112 cm, c) 4.3669 cm and d) 5.8225 cm

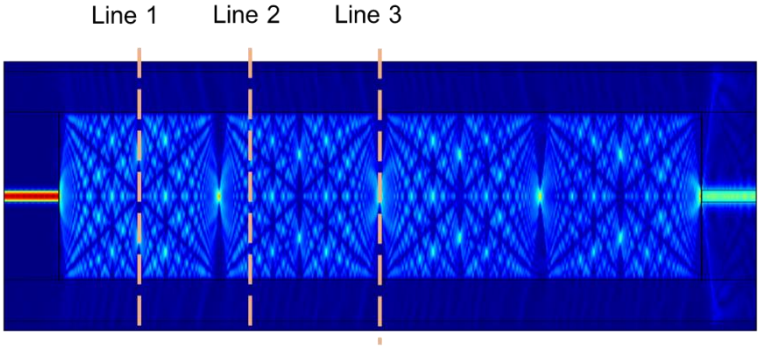

(a)

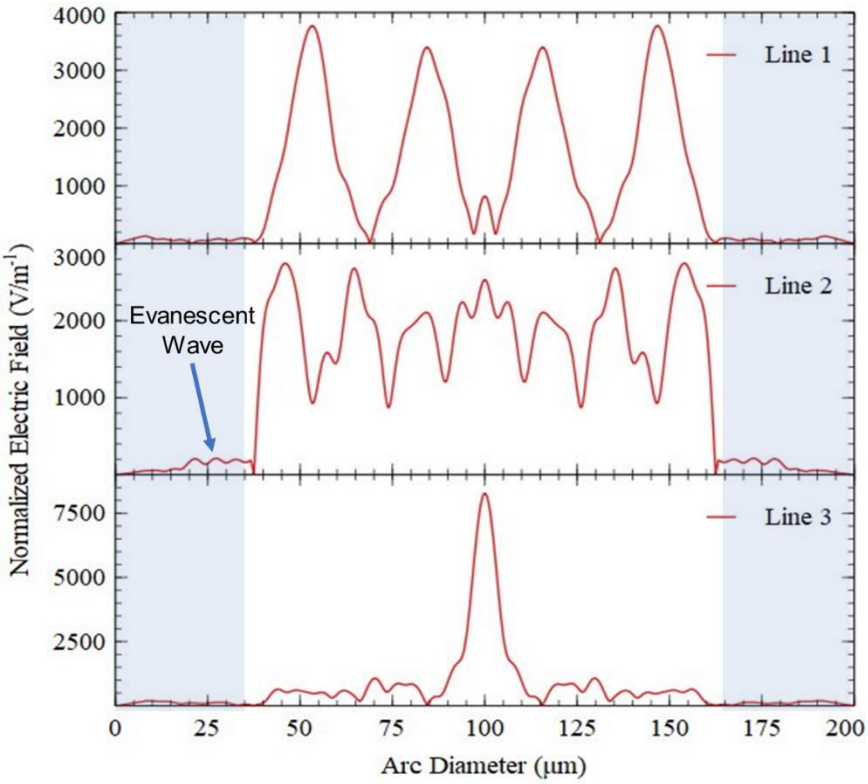

(b)

Fig. 3. (a) Light propagation and (b) mode field distribution of the NCF structure at the calculated self-image length of 5.8225 cm. The blue region indicates the analyte domain

Fig. 4 shows the enlarged image of the self-image point for one and four self-image indexes that is located at the NCF/SMF core boundary. The point is located exactly at the calculated NCF length with four decimal point, giving 0.0000 difference between the calculated and simulated length. Table 5 compares the suggested works with previous research findings. The results show that, with restricted simulation settings, the accuracy can be improved.

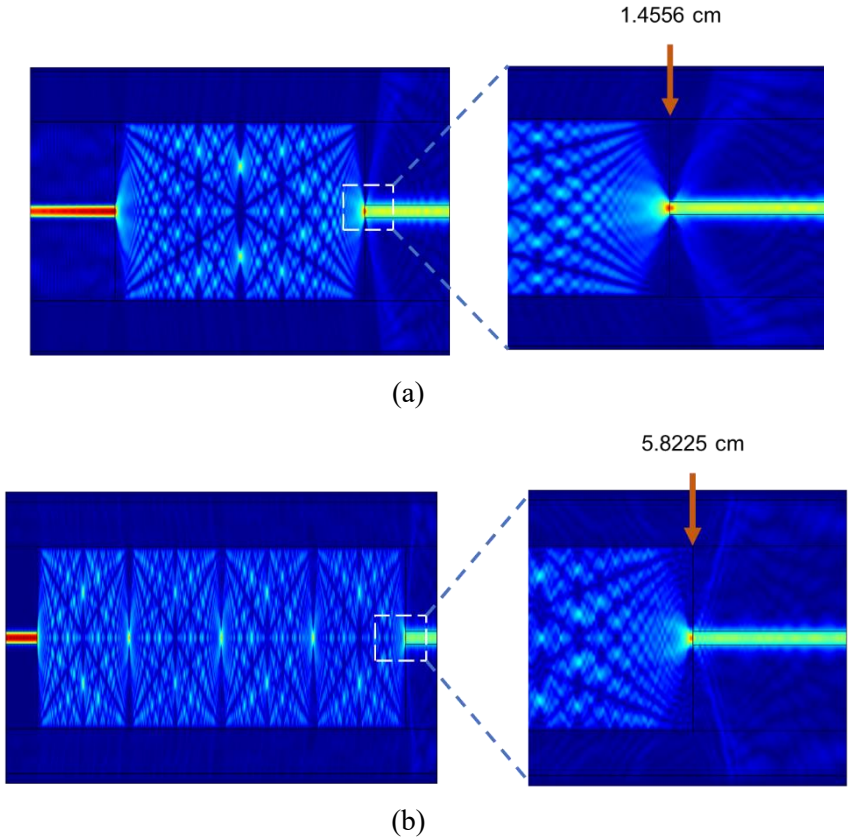

Fig. 4. Self-image point location for (a) one and (b) four self-image indexes. The point located exactly at the NCF/SMF boundary with restricted simulation settings

Table 5 Comparison study with the previous work.

Self-image index	NCF Diameter (μm)	Length from COMSOL (cm)	Length from Eq. (1) (cm)	Difference	Ref.
1	125	1.4520	1.4550	0.0030	[9]
		1.4556	1.4556	0.0000	This Work
4		5.8060	5.8220	0.1600	[9]
		5.8225	5.8225	0.0000	This Work

4. Conclusion

This work has successfully demonstrated self-image interference of the SNS by using COMSOL Multiphysics® software. The results show that, the restricted simulation settings such as PML layer and air domain has promised a good simulation illustration, improving the accuracy of the simulation results with four decimal 0.0000 difference between the theoretical calculation and simulation. The simulation settings can be used for future reference.

References

[1] Xiao, G., K. Zhang, Y. Yang, H. Yang, L. Guo, J. Li, and L. Yuan, Graphene Oxide Sensitized No-Core Fiber Step-Index Distribution Sucrose Sensor. Photonics, 2020. 7(4).
[2] Yang, W., S. Zhang, T. Geng, L. Li, G. Li, Y. Gong, K. Zhang, C. Tong, C. Lu, W. Sun, and L. Yuan, High Sensitivity Refractometer Based on a Tapered-Single Mode-No Core-Single Mode Fiber Structure. Sensors (Basel), 2019. 19(7).
[3] Sun, B., F. Li, K. Xu, K. Zhou, and Z. Zhang, Temperature-Insensitive Fiber-Optic Refractometer Based on Immobilization of Polydimethilsiloxane Film. IEEE Photonics Technology Letters, 2022. 34(3): p. 165-168.
[4] Wang, K., X. Dong, M.H. Kohler, P. Kienle, Q. Bian, M. Jakobi, and A.W. Koch, Advances in Optical Fiber Sensors Based on Multimode Interference (MMI): A Review. IEEE Sensors Journal, 2021. 21(1): p. 132-142.
[5] Bhardwaj, V., A.K. Pathak, and V.K. Singh, No-core fiber-based highly sensitive optical fiber pH sensor. J Biomed Opt, 2017. 22(5): p. 57001.
[6] Guzman-Sepulveda, J.R., R. Guzman-Cabrera, and A.A. Castillo-Guzman, Optical Sensing Using Fiber-Optic Multimode Interference Devices: A Review of Nonconventional Sensing Schemes. Sensors (Basel), 2021. 21(5).
[7] Zhao, Y., J. Zhao, and Q. Zhao, Review of no-core optical fiber sensor and applications. Sensors and Actuators A: Physical, 2020. 313: p. 112160.
[8] Antonio-Lopez, J.E., J.J. Sanchez-Mondragon, P. LiKamWa, and D.A. May-Arrioja, Fiber-optic sensor for liquid level measurement. Opt Lett, 2011. 36(17): p. 3425-7.
[9] Younus, S.I., A.A. Al-Dergazly, and A.K. Abass, Characterization of Multimode Interference Based Optical Fiber. IOP Conference Series: Materials Science and Engineering, 2021. 1076(1): p. 012060.
[10] Datta, A. and A. Saha, Manifestation of a highly sensitive evanescent wave absorption-based refractive index sensor realized by radiating with an optical Airy beam. Optical and Quantum Electronics, 2021. 53(3): p. 157.
[11] Datta, A., Enhanced sensitivity of fiber optic evanescent wave absorption-based concentration sensor by shining a Bessel–Gauss beam and effect of fiber bending on the sensor response: a theoretical analysis. Optical Engineering, 2019. 58(05): p. 1-12.
[12] Zhang, M., G. Zhu, L. Lu, X. Lou, and L. Zhu, Refractive index sensor based on ultrafine tapered single-mode nocladding single-mode fiber structure. Optical Fiber Technology, 2019. 48: p. 297-302.
[13] Khanikar, T. and V.K. Singh, Gold grating assisted SPR based D-shaped single mode fiber for detection of liquid refractive index. Optical and Quantum Electronics, 2019. 51(9): p. 296.
[14] Xu, W., J. Shi, X. Yang, D. Xu, F. Rong, J. Zhao, and J. Yao, Improved Numerical Calculation of the Single-Mode-No-Core-Single-Mode Fiber Structure Using the Fields Far from Cutoff Approximation. Sensors (Basel), 2017. 17(10): p. 2240.
[15] Malitson, I.H., Interspecimen Comparison of the Refractive Index of Fused Silica*,†. Journal of the Optical Society of America, 1965. 55(10): p. 1205-1209.
[16] Brückner, V., To the use of Sellmeier formula. Senior Experten Service (SES) Bonn and HfT Leipzig, Germany, 2011. 42: p. 242-250.
[17] Kasap, S., Optoelectronics & photonics: principles & practices: international edition. 2013:

Pearson.
[18] Chipman, R.A., W.-S.T. Lam, and G. Young, Polarized light and optical systems. 2018: CRC press.
[19] Fujiwara, E., L.E.d. Silva, H.E.d. Freitas, Y.T. Wu, and C.M.B. Cordeiro. Optical Fiber Chemical Sensor Based on the Analysis of Fiber Specklegrams Characteristics. in 2018 SBFoton International Optics and Photonics Conference (SBFoton IOPC). 2018.
[20] Fujiwara, E., L.E. da Silva, T.D. Cabral, H.E. de Freitas, Y.T. Wu, and C.M.d.B. Cordeiro, Optical Fiber Specklegram Chemical Sensor Based on a Concatenated Multimode Fiber Structure. Journal of Lightwave Technology, 2019. 37(19): p. 5041-5047.